


RESEARCH ARTICLE

High Flame Retardancy of Carbon Nanotubes Reinforced Polyelectrolyte Multilayered Nanocomposites

 Inyoung Lee¹ | Seojin Kim² | Jae-Oh Shim³ | Jung Sang Cho⁴ | Chungyeon Cho⁵ 

¹Department of Chemical Engineering, College of Engineering, Wonkwang University, Iksan, Republic of Korea | ²Department of Carbon Convergence Engineering, College of Engineering, Wonkwang University, Iksan, Jeonbuk, Republic of Korea | ³Department of Chemical Engineering/Nanoscale Environmental Sciences and Technology Institute, Wonkwang University, Iksan, Republic of Korea | ⁴Department of Engineering Chemistry, Chungbuk National University, Cheongju-si, Chungbuk, Republic of Korea | ⁵Department of Biomedical Materials Science, Jeonbuk Advanced Bio-Convergence Academy, Wonkwang University, Iksan, Jeonbuk, Republic of Korea

Correspondence: Jung Sang Cho (jscho@cbnu.ac.kr) | Chungyeon Cho (cncho37@wku.ac.kr)

Received: 29 December 2024 | **Revised:** 21 February 2025 | **Accepted:** 22 February 2025

Funding: This work was supported by the National Research Foundation of Korea (NRF) grant funded by the Korea government (MSIT) (No. RS-2024-00405537). This research was also supported by the Institute of Information and Communications Technology Planning and Evaluation (IITP)-Innovative Human Resource Development for Local Intellectualization program grant funded by the Korea government (MSIT) (IITP-2024-RS-2024-00439292).

ABSTRACT

In pursuit of multifunctional flame-retardant coatings, a layer-by-layer (LbL) assembly was used to create hybrid nanocoatings by alternating the deposition of positively charged chitosan (CH) and negatively charged sodium lignosulfonate (Lg). Carbon nanotubes (CNT), dispersed in an Lg solution, were incorporated as robust reinforcements in polymer nanocomposites. Their high aspect ratio and dense network within the CH/CNT-Lg layers resulted in coatings that were notably thicker and heavier compared to those constructed without CNT. In horizontal flame tests, the presence of CNT led to superior fire resistance. Cone calorimetry further demonstrated that incorporating CNT into a single coating completely suppressed the second peak of heat release for polyurethane foam (PUF). Additionally, total smoke release, total smoke production, maximum average rate of heat emission, and effective heat of combustion were reduced by 68.9%, 72.7%, 47.7%, and 57.3%, respectively, compared to uncoated PUF. These improvements in flame retardancy are attributed to the enhanced thermal stability and high char yields provided by CNT. Overall, given the ease of applying LbL assembly, this strategy offers a promising halogen-free approach for improving fire safety in both natural and synthetic fibers.

1 | Introduction

Commodity polymeric materials, including cotton fabrics and polyurethane foams (PUF), have been extensively utilized in home furnishings, packaging, and the automotive industry due to their low density, flexibility, and advantageous thermal and mechanical properties [1]. However, despite these advantageous characteristics, many polymeric substrates exhibit relatively low thermal stability and high flammability [2]. This susceptibility

to rapid flame spread and substantial heat release during combustion poses a critical threat to both human safety and property, highlighting the necessity for effective flame retardant (FR) solutions [3]. Traditionally, halogen-based FR materials have been the primary choice for mitigating the flammability of polymeric materials [4]. Their mechanism of action relies on the interruption of radical-chain reactions during combustion, thereby reducing both the heat release rate and flame propagation [5, 6]. Nevertheless, increasing concerns regarding the

Inyoung Lee and Seojin Kim contributed equally to this study.

toxicity of halogenated derivatives, as well as their potential to generate hazardous by-products and persistent environmental pollutants, have prompted researchers and industries to explore halogen-free FR alternatives [2, 7–9].

Eco-friendly FR composites incorporating phosphorus, boron, nitrogen, sulfur, and silica-based moieties, along with carbon skeletal structures, have gained significant attention due to regulatory mandates and environmental considerations [6, 10, 11]. When integrated into polymer matrices, these materials provide an optimal combination of flame retardancy, smoke suppression, and reduced toxicity during combustion without significantly compromising mechanical integrity [12]. Recent advances in the design of organic–inorganic hybrid nanocomposites have underscored their potential as environmentally benign FR systems by incorporating either carbon-based nanofillers or inorganic nanoparticles into polymer matrices [13, 14]. For example, carbonaceous nanomaterials such as graphene, graphene oxide, and carbon nanotubes (CNT) have emerged as promising FR additives in various polymeric substrates, owing to their inherent mechanical robustness, thermal conductivity, and superior barrier characteristics [15, 16]. The dominant flame-retarding mechanism results from reinforcing char layer formation, wherein the three-dimensionally interconnected carbon networks effectively impede heat transfer and curtail the release of flammable gases [17, 18].

Layer-by-layer (LbL) assembly has emerged as a versatile and cost-effective technique for creating structure-controlled thin films and coatings, distinguished by its relative simplicity and fine-tunable design at the nanoscale level [19, 20]. Unlike other established methods, for instance, Langmuir–Blodgett deposition or self-assembled monolayers, LbL assembly offers robust and well-ordered multilayers built through careful selection of layer constituents and chemistries [21, 22]. Various interactions, including electrostatic forces, charge transfer, hydrogen bonding, and even van der Waals attractions, facilitate the deposition of functional layers on a variety of substrates with planar, curved, or complex geometries [23, 24]. By exploiting these unique advantages of LbL assembly, researchers have used it to integrate a diverse range of nanomaterials, including polymers, carbon-based nanostructures, inorganic particulates, and biomolecules, into thin films for developing advanced multifunctional composites [25–27].

In the context of polymeric materials, the LbL assembly process has been extensively employed to impart FR properties by integrating polymers and carbon nanoparticles into a three-dimensional, multilayered structure [28–30]. Although much effort has been given to the use of CNT toward FR materials, relatively little work exists to realize highly functionalized fire-resistant CNT-based polymer nanocomposites by using LbL assembly. Despite the inherent flame-retardant benefits of CNT, their integration into polymer matrices is often hindered by issues of poor compatibility because of strong van der Waals forces and π – π interactions, which result in irreversible aggregation or restacking [31, 32]. Consequently, the performance and scalability of CNT-based materials remain limited. Recent studies have demonstrated that sonication in the presence of negatively charged polyelectrolytes effectively debundles carbon nanomaterials, mitigating reaggregation and enhancing their

dispersibility, both of which are beneficial for the development of advanced fire-resistant polymer nanocomposites via LbL assembly [33, 34].

In an effort to produce highly efficient FR materials, polymer nanocomposites, composed of CH and Lg-stabilized CNT, were fabricated via LbL assembly. The multilayered nanocomposites were systematically characterized with respect to their thickness, mass, morphology, thermal behavior, and fire-retardant performance, comparing CH/Lg and CH/CNT-Lg systems. The introduction of CNT into the polymeric matrix imparted synergistic FR enhancements, demonstrating improved fire resistance in both cotton fabrics and PUF. Such remarkable performance is attributed to the three-dimensionally interconnected network formed by carbon nanomaterials, which not only confers superior flame resistance but may also open avenues for applications requiring mechanically robust coatings and wear-resistant surfaces.

2 | Experimental Section

2.1 | Materials

Chitosan (CH, $M_w = 100,000 \text{ g mol}^{-1}$), sodium lignosulfonate (Lg, $M_w = 52,000 \text{ g mol}^{-1}$), and poly(acrylic acid) (PAA; $M_w = 100,000 \text{ g mol}^{-1}$, 35 wt% in water) were obtained from Sigma-Aldrich (Milwaukee, WI, USA). To prepare a 0.1 wt% chitosan solution, deionized (D.I) water was first adjusted to pH 2, and then chitosan powder was gradually added while stirring. After stirring overnight, the solution was brought to pH 6 before use in the LbL coating process. The pH of CH solutions was adjusted using 0.1 and 1 M HCl or NaOH purchased from Sigma-Aldrich (St. Louis, MO, U.S.A). For the anionic solution, 1 wt% Lg was dissolved in D.I. water and stirred overnight. All reagents were used as supplied, without further purification. D.I. water used throughout (resistivity $> 18.2 \text{ M}\Omega \text{ cm}$) was used in all aqueous solutions. Carbon nanotubes (CNT) with an average diameter of 13 nm, a length of approximately $12 \mu\text{m}$, and a carbon content exceeding 96 wt% were purchased from LG Chem (Daejeon, Korea). To stabilize nanotubes in water with Lg, 0.5 g of CNT was manually ground in 99.5 mL of Lg using a mortar and pestle for 15 min. The resulting mixture was then subjected to tip sonication at 45 W (Bandelin Sonopuls, Germany) in an ice-water bath for 30 min, followed by an additional 30 min of bath sonication and overnight stirring. The pH of Lg and CNT-Lg solutions was used unmodified. Silicon wafers (Si-wafers, p-type, 100, University Wafer Inc., Boston, MA) were employed as substrates for film thickness measurements and surface morphology analysis. Prior to use, the wafers were sequentially rinsed with acetone and D.I. water for 30 s each, then dried with compressed air. Ti/Au-coated 5 MHz quartz crystals (Maxtek Inc., Cypress, CA) were utilized to monitor mass uptake during the coating process. A plain-woven cotton fabric ($137 \mu\text{m}$ thick, 102 g m^{-2} , 30–40 threads· cm^{-2} ; Chungugu, Daegu, South Korea) was used for horizontal flame testing. Polyurethane foam (trade name: RJBB, density 0.027 g cm^{-3} ; JeilDeco Systems, Seoul, South Korea) was tested via cone calorimetry. A plain-woven cotton fabric ($137 \mu\text{m}$ thick, 102 g m^{-2} , 30–40 threads· cm^{-2} ; Chungugu, Daegu, South Korea) was used for horizontal flame testing. Polyurethane foam (PUF, trade name: RJBB, density

0.027 g cm⁻³; JeilDeco Systems, Seoul, South Korea) was tested via cone calorimetry.

2.2 | Layer-By-Layer Assembly

Multilayer nanocomposites were fabricated on various substrates using a Multi Dip Coater robot (Hantech Co., Daejeon, Korea). The deposition was processed in an alternating sequence of immersions in positively charged CH and negatively charged CNT-Lg solutions, with a D.I. water rinse in between each coating step. For the initial bilayer (BL), substrates were immersed in the CH solution for 5 min, followed by a 5 min dip in the CNT-Lg suspension, and each immersion was succeeded by a 1 min D.I. water rinse. After forming the first BL, the dipping time for subsequent CH and CNT-Lg cycles was reduced to 1 min each. This process was repeated until the desired number of BLs was achieved. When coating three-dimensional substrates such as cotton fabric or PUF, a primer step was introduced by soaking the samples for 5 min in a 1.0 wt% PAA solution at pH 2 (adjusted with 2 M HNO₃) prior to the LbL assembly. Following the final deposition cycle, all coated samples were air-dried overnight at ambient conditions before further analysis and testing.

2.3 | Thin Film Characterization

The thickness of the multilayer thin films assembled on silicon wafers was evaluated using a NanoMap-PS contact-mode stylus profilometer (Aeptechnology, Santa Clara, CA, USA). Thickness data were averaged from five measurements taken at different locations on each of three independent samples. A QCM200 quartz crystal microbalance (Stanford Research Systems Inc., Sunnyvale, CA, USA) provided the mass increment of each deposited component on the sensor surface. Surface morphology was examined by atomic force microscopy (AFM, Nanostation IITM, Surface Imaging Systems, Herzogenrath, Germany) and S-4800 field-emission scanning electron microscopy (FE-SEM, Hitachi, Japan). UV-vis absorbance spectra of films on

glass slides were obtained using a Shimadzu UV-1900 spectrophotometer (Shimadzu, Japan), and Fourier transform infrared spectra were recorded on an FT-IR 680 plus spectrometer (JASCO, Japan).

2.4 | Flame Retardant Characterization

Thermal stability of both uncoated and coated PUF samples was assessed using a Q-50 thermogravimetric analyzer (TGA, TA Instruments, New Castle, DE, USA). Each sample (approximately 20 mg) was heated from room temperature to 800°C under nitrogen flow at a rate of 5°C min⁻¹. Horizontal flame testing (HFT) was conducted on cotton fabrics (10 × 32 cm²) placed in a U-shaped metal frame, following ASTM D5132 guidelines (AD-HV09, ADE, Korea). Cone calorimetry measurements were performed in accordance with ISO 5660-1, using cuboid specimens (10 × 10 × 2.5 cm³) mounted in an aluminum foil tray and exposed to a heat flux of 35 kW m⁻² in a horizontal orientation. Other fire performance parameters such as heat release rate (HRR), total smoke release (TSR), total smoke production (TSP), maximum average rate of heat emission (MARHE), and effective heat of combustion (EHC) were recorded to evaluate the FR properties of uncoated and coated PUF. In addition, the fire resistance of PUF and wood samples was examined by applying a direct butane torch flame (approximately 1200°C) to observe the protective behavior of the multilayer nanocomposite coatings under extreme conditions.

3 | Results and Discussion

Multilayered nanocomposites were fabricated by immersing a substrate in cationic CH followed by immersion in an anionic Lg-based dispersion, either with or without CNT, as illustrated in Figure 1a,b. To create a flame-suppressing coating on cotton textiles and PUF, a 1 wt% PAA layer was first applied to enhance interlayer adhesion. The subsequent assembly of CH/Lg layers was achieved by alternatively dipping the substrate

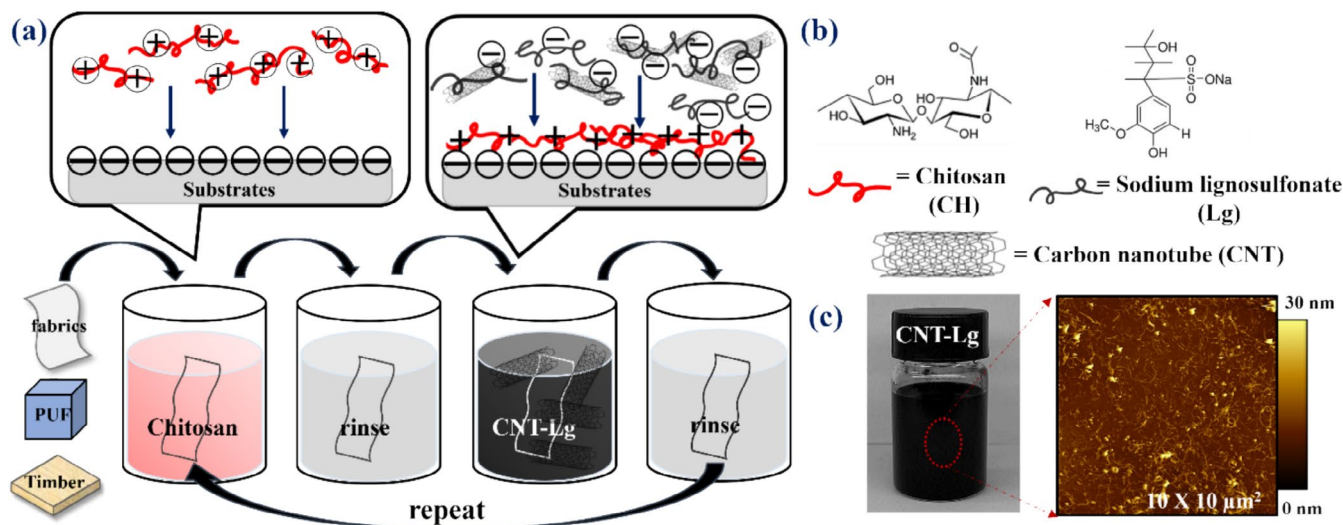


FIGURE 1 | Schematics of layer-by-layer assemblies on various substrates such as cotton fabrics, PUF, and timbers; (b) chemical structures of CH, Lg, and CNT used in this study; and (c) optical image of CNT-Lg and its corresponding AFM image. [Color figure can be viewed at [wileyonlinelibrary.com](https://onlinelibrary.wiley.com/doi/10.1002/aps.56967)]

into positively charged CH and negatively charged Lg, utilizing electrostatic interactions to form stable BLs. Because CNT can serve as effective flame retardant additives, ensuring their uniform dispersion is crucial. Aggregation resulting from strong van der Waals forces among these hydrophobic, nanoscale materials can significantly compromise the overall performance of the polymer nanocomposites [35]. In this study, uniformly dispersed CNT in aqueous Lg, as shown in Figure 1c, demonstrates that the black-colored nanotubes can be stably suspended without noticeable precipitation. AFM images of samples prepared from dilute solutions further confirmed well-dispersed nanotubes by Lg in water.

3.1 | Film Growth

The multilayer formation of polymer nanocomposite assembly in terms of films thickness was examined using a stylus profilometer. As shown in Figure 2a, both CH/Lg and CH/CNT-Lg layers exhibited a linear increase in thickness with the number of deposited layers on Si wafers, indicating uniform deposition. The average thickness per BL was measured as 4.2 nm for CH/Lg and 15.5 nm for CH/CNT-Lg. The substantially higher thickness observed for the CH/CNT-Lg system is attributed to the inclusion of CNT, which introduces a three-dimensional network. In addition, quartz crystal microbalance (QCM) analyses (Figure 2b) revealed that the mass in both coating systems displayed a linear increment with the number of deposition cycles, suggesting that the composition remains consistent at each step. Notably, CH/CNT-Lg showed an average mass increase per BL of $2.19 \mu\text{g cm}^{-2}$, which is roughly 4.7 times greater than that for CH/Lg ($0.46 \mu\text{g cm}^{-2}$). By correlating these mass growth measurements with the thickness data, the densities of CH/Lg and CH/CNT-Lg films were estimated to be 0.97 and 1.41 g cm^{-3} , respectively. The higher density of CH/CNT-Lg is likely due to the incorporation of CNT, forming a more tightly packed structure.

The multilayer formation was examined by using UV-vis spectroscopy. Both LbL thin films exhibited a characteristic absorption peak at 280 nm that indicates the presence of CH and Lg (Figure S1a) [36]. The CNTs-containing nanocomposites

displayed a more distinct peak relative to CH/Lg. Such an intense peak in the CH/CNT-Lg systems can be explained as follows: The strong π -conjugated electronic transition properties of carbon nanotubes, combined with electronic/chemical interactions between the polymers and nanotubes, as well as an increase in surface area due to effective dispersion, collectively lead to stronger UV-vis absorption peaks in polymer composites containing carbon nanotubes. FT-IR spectra of both systems exhibited the characteristic bands of each component; a peak at 1570 nm is indicative of N-H bending vibrations from both the amide group and the deacetylated primary amine group present in chitosan (Figure S1b) [37]. The characteristic peaks at 1590, 1420, 1170, and 650 nm correspond to the carbonyl ion (COO^-), aromatic skeleton vibration ($\text{C}=\text{C}$ bonds), $\text{O}=\text{S}=\text{O}$ in SO_3^- (sodium salts), and the S-O band of sodium lignosulfonate, respectively [38, 39]. The UV-vis and FT-IR analyses clearly confirm the successful deposition of each component into the film.

3.2 | Multilayer Structure

Morphological features of nanocomposite thin films prepared via layer-by-layer (LbL) assembly were investigated using AFM and SEM, as shown in Figure 3. The two types of films exhibited distinctly different surface structures. The CH/Lg multilayers presented a smooth and homogeneous surface (Figure 3a). In contrast, AFM images of 3 BL CH/CNT-Lg composite films on silicon wafers revealed a dense coverage of nanotubes across the top layer (Figure 3c). Quantitative roughness analysis from $10 \times 10 \mu\text{m}^2$ AFM scans indicated that the root-mean-square (rms) surface roughness of CH/CNT-Lg films (12.1 nm) was significantly higher than that of CH/Lg films without CNT (3.4 nm). This pronounced increase in roughness can be attributed to the entangled nanotube networks formed on the film surface. SEM observations further confirmed these findings. While the CH/Lg films showed a relatively featureless, uniform surface, the inclusion of CNT yielded a random and homogeneous dispersion of nanotubes, resulting in a visibly entangled nanotube network. This morphological contrast emphasizes the role of CNT incorporation in modifying both the topographical and structural properties of LbL-assembled nanocomposite thin films.

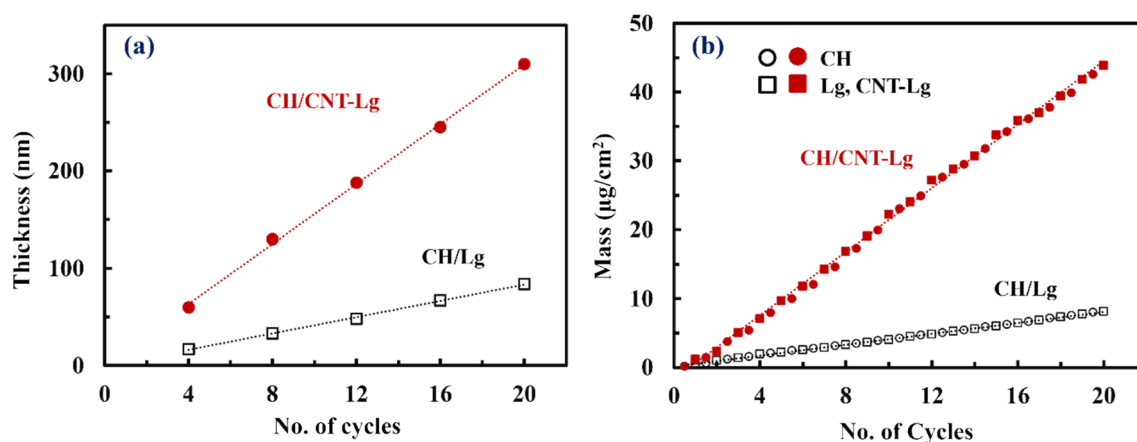


FIGURE 2 | (a) Film thickness and (b) mass of CH/Lg and CH/CNT-Lg versus the number of bilayers deposited. [Color figure can be viewed at [wileyonlinelibrary.com](https://onlinelibrary.wiley.com)]

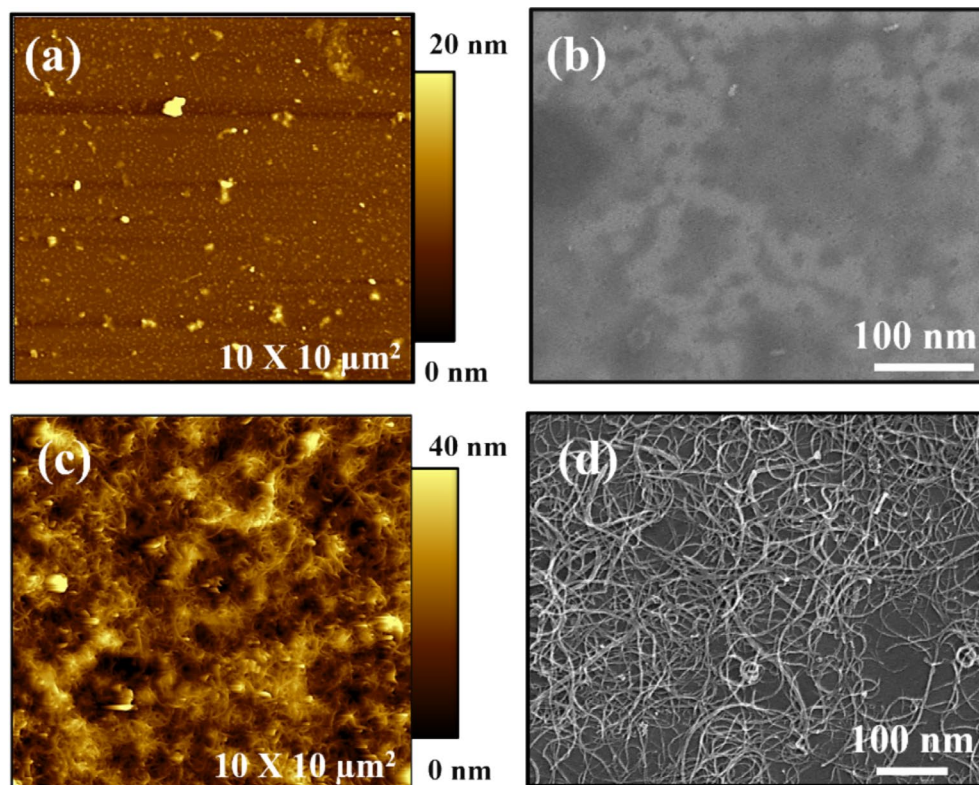


FIGURE 3 | AFM phase images of (a) 3 BL CH/Lg and (c) CH/CNT-Lg thin films. SEM surface images of (b) 3 BL CH/Lg and (d) CH/CNT-Lg assemblies. [Color figure can be viewed at [wileyonlinelibrary.com](https://onlinelibrary.wiley.com)]

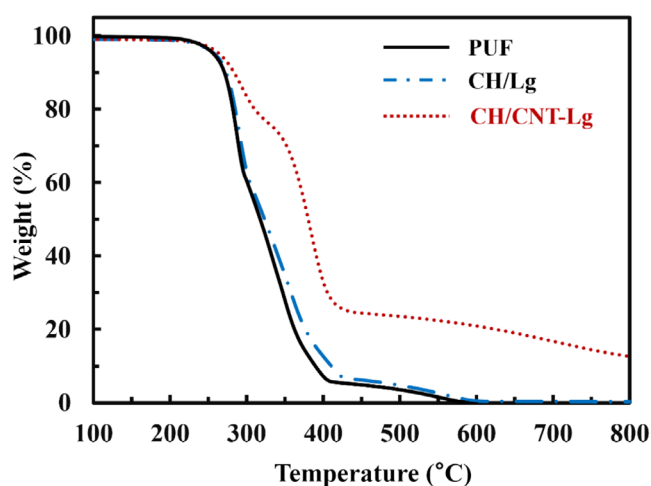


FIGURE 4 | Weight versus temperature for uncoated PUF and 20 BL CH/Lg and CH/CNT-Lg assemblies coated on PUF. TGA analysis on each sample was performed at a heating rate of 5°C min⁻¹ in the nitrogen gas condition. [Color figure can be viewed at [wileyonlinelibrary.com](https://onlinelibrary.wiley.com)]

3.3 | Thermal Stability

Figure 4 displays TGA results obtained under a nitrogen atmosphere for PUF samples, both uncoated and coated. The deposition method was analogous to that used for flat substrates such as Si wafers; however, the PUF was manually wrung after each coating step to remove excess solution. Following the LbL assembly, the foams were air-dried prior to TGA measurements.

The weight percentage of residue was monitored with increasing temperature, and no significant difference in the initial degradation profile was observed for uncoated versus coated PUF up to approximately 270°C. Beyond this point, the control foam began to show a distinct degradation trend. In agreement with previous reports, the thermal breakdown of PUF generally proceeds through two stages: the first at around 270°C, involving degradation of hard segments into isocyanates, alcohols, amines, olefins, and carbon dioxide, and the second near 410°C, corresponding to the decomposition of soft (polyol) segments [40, 41]. By around 560°C, the uncoated foam was almost fully degraded, leaving negligible residue. By comparison, the CH/Lg-coated PUF exhibited a similar overall degradation curve, retaining around 0.3 wt% residue at 600°C. However, the 20-bilayer CH/CNT-Lg-coated foam demonstrated considerably enhanced thermal stability, with the final residue reaching 17.1 wt% at 700°C, when the baseline contribution of the coating-free sample was taken into account. This enhanced char yield, arising from nanotube incorporation, underscores the potential of CNT-based nanocomposite coatings for improving fire resistance in polymeric materials.

3.4 | Flame Retardant Behavior

Multilayered nanocomposite coatings were deposited onto cotton fabrics following a procedure similar to that used for Si wafers and quartz crystals. The coating add-on was quantified by calculating the weight gain (add-on, % = $(W - W_0)/W_0 \times 100\%$), where W_0 is the initial fabric mass and W is the mass after deposition of the desired number of layers (Table S1). As expected,

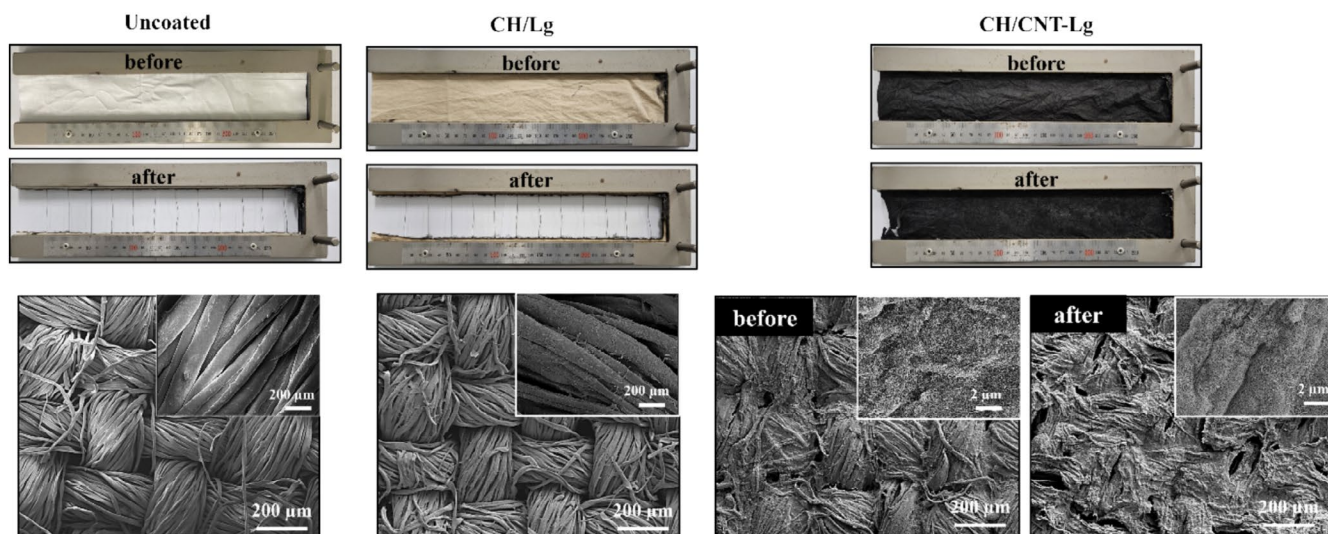


FIGURE 5 | Photographs (top) of fabrics before and after horizontal flame tests (HFT) and SEM images (bottom) of fabrics before and after HFT of uncoated and 20 BL CH/Lg and CH/CNT-Lg-coated fabrics. The inset images at high magnification show the smooth surface of pristine fabrics and the LbL-based structure deposited on the fabric surface. [Color figure can be viewed at [wileyonlinelibrary.com](https://onlinelibrary.wiley.com)]

the overall weight gain increased with the number of deposition cycles and was more pronounced for the CNT-containing systems, indicating higher loading of constituents. To evaluate fire performance, horizontal flame testing (HFT) was carried out on coated and uncoated fabrics. Both the uncoated control and the CH/Lg-coated samples were completely consumed, leaving no visible residue on the sample holder (Figure 5, left and middle, top row, and Videos S1 and S2). The cotton fabrics coated with fewer layers (such as 5–10 bilayers) were also tested. These samples were completely consumed, leaving no visible residue on the sample holder (Figure S3 in the Supporting Information). In contrast, the 20-bilayer CH/CNT-Lg coatings exhibited substantial char formation (Figure 5, right, top row; Video S3), which not only remained intact but also preserved the integrity of the underlying fabric. This result highlights the critical role of CNT incorporation in enhancing the FR properties of LbL assemblies on textile substrates.

Scanning electron microscopy (SEM) was employed to evaluate the surface architecture and morphological changes of both uncoated and LbL-coated fabrics before and after HFT, as depicted in Figure 5 (bottom). Prior to flame exposure, the uncoated control displayed a relatively uniform, smooth surface compared to the coated samples. Conversely, the CH/Lg-coated fabrics showed an uneven surface morphology, potentially due to polyelectrolyte aggregation on individual fibers, which is likely a consequence of inefficient rinsing during the deposition process. The presence of CNT imparted a distinctly rough texture to the coating, with higher magnification images confirming extensive nanotube coverage on each fiber, indicating successful CNT integration into the multilayer assembly. Post-HFT SEM images for the control and CH/Lg-coated fabrics were not included since these samples were fully consumed during the burn test. In contrast, the CNT-containing coatings maintained the overall woven structure, although the surface appeared relatively smooth, probably as a result of thermal fusion of the nanocomposite layers during flammability testing. Higher magnification micrographs revealed that individual fibers in the

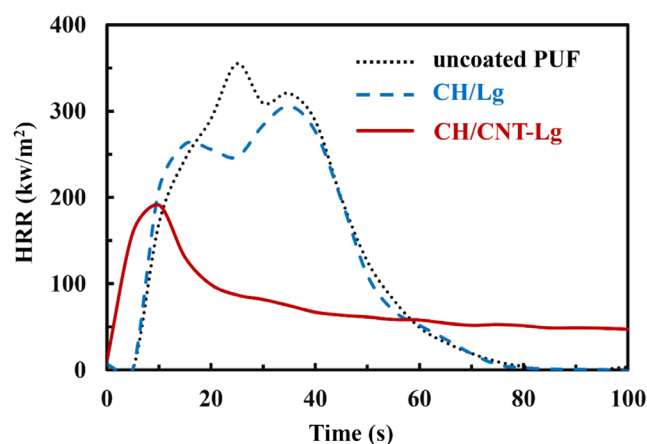


FIGURE 6 | Heat-release rate (HRR), as a function of time, during cone calorimeter testing for uncoated control and 20-BL multilayers-coated polyurethane foam (PUF). [Color figure can be viewed at [wileyonlinelibrary.com](https://onlinelibrary.wiley.com)]

CNT-coated fabrics retained nanotube networks even after exposure to flames, underscoring the robustness of these coatings under high-temperature conditions.

To more quantitatively evaluate the coatings' effectiveness as a thermal barrier, cone calorimetry was carried out on both uncoated and LbL-coated PUF samples. The heat release rate (HRR), a key indicator of flammability, was recorded over time (Figure 6). Additional cone calorimetry data, including total heat release (THR), total smoke production (TSP), maximum average rate of heat emission (MARHE), and effective heat of combustion (EHC), are presented in Table S2. Under an applied heat flux of 35 kW m^{-2} , the control PUF exhibited two distinct HRR peaks. The first, appearing at 25 s (351.1 kW m^{-2}), corresponds to foam collapse driven by the PUF's low thermal conductivity, leading to a rapid temperature rise at the surface, and is attributed to polyisocyanate pyrolysis. The second peak at 35 s (320.2 kW m^{-2}) is associated with the breakdown of soft

segments deriving from the polyol component. When 20 BL of CH/Lg were deposited onto the foam, these initial and secondary peak HRRs were reduced to 261.2 and 305.6 kW m⁻², respectively, representing declines of 25.6% and 4.6% in comparison with the uncoated PUF.

The 20 BL CH/CNT-Lg coating with an approximate thickness of 310 nm substantially reduced the flammability of PUF. Compared to the uncoated control, the first peak heat release rate (pkHRR) dropped by 45.4% (191.6 kW m⁻²), and the second HRR peak was entirely suppressed. In addition, this coating led to marked decreases in total smoke release (TSR), total smoke production (TSP), maximum average rate of heat emission (MARHE), and effective heat of combustion (EHC) by 68.9%, 72.7%, 47.7%, and 57.3%, respectively (Table S2), surpassing the reductions observed for polymer-only multilayer coatings (65.1%, 66.7%, 49.6%, and 53.9%, respectively). These cone calorimetry results indicate that introducing CNT into the multilayer system provides a more robust barrier against heat transfer than coatings made solely from polymers. A higher HRR at longer time scales was observed in the CNT-based nanocomposites. This is likely explained by the ability of CNT-containing coatings to reduce heat transfer from the flame front, thereby delaying combustion and consequently elevating the HRR over time. Moreover, these nanocomposites promote the formation of a protective char layer on the surface, which insulates the underlying foam from heat and flames, potentially leading to increased HRR during the later stages of char formation.

To further evaluate FR performance, a 12-s torch flame test was conducted on the coated foam to precisely assess its fire resistance. Under direct flame, the uncoated foam rapidly melted, released thick smoke, and exhibited severe dripping, potentially causing additional hazards (Video S4). These observations highlight the foam's limited fire stability in its untreated state. Although applying a CH/Lg coating prevented dripping, the foam substrate was still entirely consumed, leaving no residue (Video S5). In contrast, incorporating CNT into the nanocoating significantly enhanced flame suppression. The 20 bilayer CH/CNT-Lg coating not only limited dripping but also preserved the foam's structural integrity despite partial decomposition

(Video S6). Cross-sectional inspection of the CNT-coated foam revealed that most of the interior remained intact beneath the char layer, with around 70 wt% mass retained.

A representative photograph and SEM image of the uncoated PUF (Figure 7) highlight its characteristic three-dimensional network of open pores, featuring smooth cell walls. After coating with the CH/CNT-Lg system, the foam retained its original macroscopic porosity and cell dimensions while displaying extensive coverage of the open cellular structure. Higher-magnification micrographs revealed that individual pore surfaces were conformally coated by the nanotubes, suggesting successful LbL deposition. Moreover, an SEM image at the interface between the remaining char and the underlying foam, captured post-torch testing, indicated that the foam preserved its shape. Under high magnification, it was evident that the char consisted of densely packed nanotubes.

For a more industry-oriented demonstration, the 20 BL nanocomposite coating was applied to 4-mm-thick birch panels via a spray-coating process, with the substrates placed 15 cm from the sprayer and each component sprayed for 20 s without rinsing. Upon exposing the uncoated and CH/Lg-coated wood to a butane torch flame for 1 min, nearly the entire birch sample was consumed after flame extinction (Figure S3 and Videos S7 and S8). In contrast, the CH/CNT-Lg-coated wood self-extinguished within 2 s after the flame was removed, retaining its structure (Video S9). This halogen-free flame-retardant (FR) coating shows promise for safeguarding timber used in building applications, thereby enhancing overall safety in modern construction. Indeed, incorporating flame-retardant wooden components can significantly reduce the risk of fire spread while preserving the natural aesthetics and sustainability of wood. Moreover, the improved thermal stability facilitated by these CNT-based nanocoatings extends the potential use of wood into more demanding structural or decorative contexts in architectural design. A well-known limitation of traditional dip-based LbL processes is the prolonged deposition time, as well as the substantial number of layers required to achieve specific properties. In the present study, we adopted a spray-based LbL approach to deposit coatings on wood substrates. By selecting

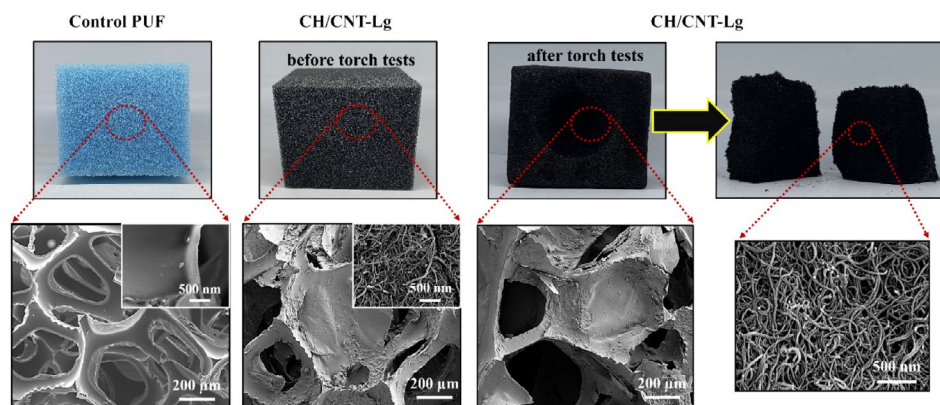


FIGURE 7 | Photographs (top row) and SEM (bottom row) images of neat polyurethane foam (PUF) and 20 BL CH/CNT-Lg coated PUF samples before and after torch tests. The inset SEM images at high magnification show a pristine foam and CNT-deposited structure. [Color figure can be viewed at [wileyonlinelibrary.com](https://onlinelibrary.wiley.com)]

this method, our objective was to design a more efficient system, achieving enhanced performance with fewer layers, and thus reducing processing time. The flame-retardant properties achieved in our work are comparable to those reported for other LbL coatings in the literature (Table S3).

The present study demonstrates an efficient FR coating system with relatively few layers in which nanometer-thick CNTs are integrated into eco-friendly polymer-based multilayer nanocomposites. TGA and a variety of flame testing methods, including HFT, torch tests, and cone calorimetry, collectively confirm that CNT incorporation markedly enhances fire resistance. By embedding nanotubes into polymer-based coatings, the underlying polymer substrate gains improved thermal protection, effectively mitigating heat transfer and significantly boosting overall fire safety [18]. The entangled CNT network functions as a heat shield, reducing the rate of heat conduction into the underlying substrate [42]. Moreover, CNTs can act as physical barriers that slow down the diffusion of volatile degradation products, thereby delaying the onset of pyrolysis in cotton and PUF [43, 44]. An improved FR behavior in this system is closely associated with the char-forming ability of CNT-based polymer composites. Under high heat flux, the polymeric matrix around the CNTs begins to degrade, and the nanotubes help reinforce the carbonized residue, creating a thermally robust, cohesive char [28, 45–47]. This char layer insulates the substrate from further degradation by limiting oxygen diffusion and blocking radiant heat transfer. Although more layers often yield better flame retardancy (e.g., lower heat release rate, higher limited oxygen index, improved char formation), the improvements eventually begin to level off. This “plateau” occurs because, once a certain level of coverage or active species has been deposited, the incremental benefit of additional layers becomes quite small compared to the extra weight, processing time, and cost. Consequently, we believe that the 20-bilayer coating in the present work represents an “optimal number” of bilayers that balances strong FR performance with acceptable processing time, mechanical properties, and overall cost.

4 | Conclusion

In this study, eco-friendly polymer-based nanocomposites were assembled using an LbL approach to confer flame retardancy to various polymeric substrates, such as cotton fabrics and PUF. The incorporation of CNT proved highly effective, as demonstrated by cone calorimetry measurements that revealed the complete suppression of the second heat release rate peak and significant reductions in TSR, TSP, MARHE, and EHC for the CNT-containing coatings. These improvements were attributed to the CNT network, which facilitates the formation of char layers capable of mitigating both heat and mass transfer, an observation further supported by TGA. Integrating CNT into polymer-based multilayers could be an excellent strategy for imparting flame retardancy to both natural and synthetic fibers. CNT-loaded polymer nanocomposite coatings offer superior fire-resistant performance while maintaining efficient, straightforward manufacturing processes, representing a promising pathway toward safer, more thermally stable materials in a broad range of applications.

Author Contributions

Inyoung Lee: conceptualization (equal), data curation (equal), formal analysis (equal), methodology (equal), writing – original draft (equal). **Seojin Kim:** conceptualization (equal), data curation (equal), investigation (equal), writing – original draft (equal). **Jae-Oh Shim:** conceptualization (equal), data curation (equal), resources (equal), supervision (equal). **Jung Sang Cho:** conceptualization (equal), investigation (equal), writing – original draft (equal), writing – review and editing (equal). **Chungyeon Cho:** data curation (lead), funding acquisition (lead), investigation (lead), supervision (lead), writing – original draft (lead), writing – review and editing (lead).

Acknowledgments

This work was supported by the National Research Foundation of Korea (NRF) grant funded by the Korea government (MSIT) (No. RS-2024-00405537). This research was also supported by the Institute of Information and Communications Technology Planning and Evaluation (IITP)-Innovative Human Resource Development for Local Intellectualization program grant funded by the Korea government (MSIT) (IITP-2024-RS-2024-00439292).

Data Availability Statement

The data that support the findings of this study are available from the corresponding author upon reasonable request.

References

1. H. Yang, B. Yu, P. Song, C. Maluk, and H. Wang, “Surface-Coating Engineering for Flame Retardant Flexible Polyurethane Foams: A Critical Review,” *Composites Part B: Engineering* 176 (2019): 107185.
2. A. Dasari, Z.-Z. Yu, G.-P. Cai, and Y.-W. Mai, “Recent Developments in the Fire Retardancy of Polymeric Materials,” *Progress in Polymer Science* 38 (2013): 1357–1387.
3. M. Liu, J. Qiao, X. Zhang, et al., “Flame Retardant Strategies and Applications of Organic Phase Change Materials: A Review,” *Advanced Functional Materials* 35 (2024): 2412492.
4. H. Feuchter, F. Poutch, and A. Beard, “The Impact of Halogen Free Phosphorus, Inorganic and Nitrogen Flame Retardants on the Toxicity and Density of Smoke From 10 Common Polymers,” *Fire and Materials* 47 (2023): 1003–1023.
5. A. B. Morgan and J. W. Gilman, “An Overview of Flame Retardancy of Polymeric Materials: Application, Technology, and Future Directions,” *Fire and Materials* 37 (2013): 259–279.
6. M. Kianfar, H. Ipakchi, S. Mohajer, et al., “Flame-Retardant Self-Healing Polymers: A Review,” *Journal of Polymer Science* (2024).
7. M. Sabet, “Advancements in Halogen-Free Polymers: Exploring Flame Retardancy, Mechanical Properties, Sustainability, and Applications,” *Polymer-Plastics Technology and Materials* 63 (2024): 1794–1818.
8. S. Agnihotri, J. N. Sheikh, S. Singh, and B. Behera, “Flame-Retardant Textile Structural Composites for Construction Application: A Review,” *Journal of Materials Science* 59 (2024): 1788–1818.
9. A. Mouren and L. Avérous, “Sustainable Cycloaliphatic Polyurethanes: From Synthesis to Applications,” *Chemical Society Reviews* 52 (2023): 277–317.
10. I. Lee, J. Kim, S. Yun, et al., “Synergistic Combination of Dual Clays in Multilayered Nanocomposites for Enhanced Flame Retardant Properties,” *ACS Omega* 9 (2024): 6606–6615.
11. A. Yadav, F. M. de Souza, T. Dawsey, and R. K. Gupta, “Recent Advancements in Flame-Retardant Polyurethane Foams: A Review,” *Industrial and Engineering Chemistry Research* 61 (2022): 15046–15065.

12. G. H. Yeoh, I. M. De Cachinho Cordeiro, W. Wang, et al., "Carbon-Based Flame Retardants for Polymers: A Bottom-up Review," *Advanced Materials* 36 (2024): 2403835.
13. S. Araby, B. Philips, Q. Meng, J. Ma, T. Laoui, and C. H. Wang, "Recent Advances in Carbon-Based Nanomaterials for Flame Retardant Polymers and Composites," *Composites Part B: Engineering* 212 (2021): 108675.
14. I. Lee, J. Jang, D. Choi, Y. T. Park, and C. Cho, "Layer-by-Layer Assembly of TiO₂ Nanoparticle/Poly (acrylic acid)/Montmorillonite Trilayer Composite Films as Flame-Retardant Coatings," *ACS Applied Nano Materials* 7 (2024): 26843.
15. R. Gupta, M. K. Singh, S. M. Rangappa, S. Siengchin, H. N. Dhakal, and S. Zafar, "Recent Progress in Additive Inorganic Flame Retardants Polymer Composites: Degradation Mechanisms, Modeling and Applications," *Heliyon* 10 (2024): e39662.
16. J. Kim, J. Jang, S. Yun, et al., "Synergistic Flame Retardant Effects of Carbon Nanotube-Based Multilayer Nanocoatings," *Macromolecular Materials and Engineering* 306 (2021): 2100233.
17. G. Beyer, "Short Communication: Carbon Nanotubes as Flame Retardants for Polymers," *Fire and Materials* 26 (2002): 291–293.
18. A. Kausar, I. Rafique, and B. Muhammad, "Significance of Carbon Nanotube in Flame-Retardant Polymer/CNT Composite: A Review," *Polymer-Plastics Technology and Materials* 56 (2017): 470–487.
19. J. J. Richardson, M. Björnalm, and F. Caruso, "Technology-Driven Layer-By-Layer Assembly of Nanofilms," *Science* 348, no. 6233 (2015): aaa2491, <https://doi.org/10.1126/science.aaa2491>.
20. J. Borges and J. F. Mano, "Molecular Interactions Driving the Layer-By-Layer Assembly of Multilayers," *Chemical Reviews* 114 (2014): 8883–8942.
21. J. J. Richardson, J. Cui, M. Björnalm, J. A. Braunger, H. Ejima, and F. Caruso, "Innovation in Layer-By-Layer Assembly," *Chemical Reviews* 116 (2016): 14828–14867.
22. X. Zhang, Y. Xu, X. Zhang, et al., "Progress on the Layer-By-Layer Assembly of Multilayered Polymer Composites: Strategy, Structural Control and Applications," *Progress in Polymer Science* 89 (2019): 76–107.
23. K. Ariga, Y. Lvov, and G. Decher, "There Is Still Plenty of Room for Layer-by-Layer Assembly for Constructing Nanoarchitectonics-Based Materials and Devices," *Physical Chemistry Chemical Physics* 24 (2022): 4097–4115.
24. S. Zhang, F. Xia, S. Demoustier-Champagne, and A. M. Jonas, "Layer-By-Layer Assembly in Nanochannels: Assembly Mechanism and Applications," *Nanoscale* 13 (2021): 7471–7497.
25. C. Wang, M. J. Park, H. Yu, H. Matsuyama, E. Drioli, and H. K. Shon, "Recent Advances of Nanocomposite Membranes Using Layer-By-Layer Assembly," *Journal of Membrane Science* 661 (2022): 120926.
26. J. Zeng and M. Matsusaki, "Layer-By-Layer Assembly of Nanofilms to Control Cell Functions," *Polymer Chemistry* 10 (2019): 2960–2974.
27. W. Yuan, G.-M. Weng, J. Lipton, C. M. Li, P. R. Van Tassel, and A. D. Taylor, "Weak Polyelectrolyte-Based Multilayers via Layer-By-Layer Assembly: Approaches, Properties, and Applications," *Advances in Colloid and Interface Science* 282 (2020): 102200.
28. X. Qiu, Z. Li, X. Li, and Z. Zhang, "Flame Retardant Coatings Prepared Using Layer by Layer Assembly: A Review," *Chemical Engineering Journal* 334 (2018): 108–122.
29. C.-H. Xue, Y. Wu, X.-J. Guo, B.-Y. Liu, H.-D. Wang, and S.-T. Jia, "Superhydrophobic, Flame-Retardant and Conductive Cotton Fabrics via Layer-By-Layer Assembly of Carbon Nanotubes for Flexible Sensing Electronics," *Cellulose* 27 (2020): 3455–3468.
30. Q. Liu, S. Gao, Y. Zhao, W. Tao, X. Yu, and M. Zhi, "Review of Layer-By-Layer Self-Assembly Technology for Fire Protection of Flexible Polyurethane Foam," *Journal of Materials Science* 56 (2021): 9605–9643.
31. M. Zafar, S. M. Imran, I. Iqbal, et al., "Graphene-Based Polymer Nanocomposites for Energy Applications: Recent Advancements and Future Prospects," *Results in Physics* 60 (2024): 107655.
32. L. Qiao and K. Du, "Scalable Production of High-Quality Carbon Nanotube Dispersion in Aqueous Solution Using Cellulose as Dispersant by a Freezing/Thawing Process," *Journal of Colloid and Interface Science* 623 (2022): 1200–1209.
33. Y.-y. Byun, J. Jang, M. Culebras, et al., "Conformation-Dependent Thermoelectric Power Factor of Multilayer Nanocomposites," *Applied Surface Science* 594 (2022): 153483.
34. C. Cho, M. Culebras, K. L. Wallace, et al., "Stable n-Type Thermoelectric Multilayer Thin Films With High Power Factor From Carbonaceous Nanofillers," *Nano Energy* 28 (2016): 426–432.
35. C. I. Idumah and C. M. Obele, "Understanding Interfacial Influence on Properties of Polymer Nanocomposites," *Surfaces and Interfaces* 22 (2021): 100879.
36. D. Rani, B. Nayak, and S. Srivastava, "Smaller Sized Hepatitis E Virus ORF2 Protein-Chitosan Nanoemulsion Conjugate Elicits Improved Immune Response," *Biointerface Research in Applied Chemistry* 13 (2023): 46.
37. S. Bandara, C.-a. Carnegie, C. Johnson, et al., "Synthesis and Characterization of Zinc/Chitosan-Folic Acid Complex," *Heliyon* 4, no. 8 (2018): e00737, <https://doi.org/10.1016/j.heliyon.2018.e00737>.
38. E. A. Karpukhina, D. S. Volkov, and M. A. Proskurnin, "Quantification of Lignosulfonates and Humic Components in Mixtures by ATR FTIR Spectroscopy," *Agronomy* 13 (2023): 1141.
39. E. S. Wibowo and B.-D. Park, "Chemical and Thermal Characteristics of Ion-Exchanged Lignosulfonate," *Molecules* 28 (2023): 2755.
40. R. H. Kraemer, M. Zammarano, G. T. Linteris, U. W. Gedde, and J. W. Gilman, "Heat Release and Structural Collapse of Flexible Polyurethane Foam," *Polymer Degradation and Stability* 95 (2010): 1115–1122.
41. I. Lee, S. J. Kim, Y. Y. Byun, et al., "High Flame Retardancy Enabled by Dual Clays-Based Multilayer Nanocomposites," *Progress in Organic Coating* 183 (2023): 107784.
42. Y. Yang, J. L. Díaz Palencia, N. Wang, Y. Jiang, and D.-Y. Wang, "Nanocarbon-Based Flame Retardant Polymer Nanocomposites," *Molecules* 26 (2021): 4670.
43. R. Giri, L. Nayak, and M. Rahaman, "Flame and Fire Retardancy of Polymer-Based Composites," *Materials Research Innovations* 25 (2021): 104–132.
44. W. Xing, W. Yang, W. Yang, et al., "Functionalized Carbon Nanotubes With Phosphorus-and Nitrogen-Containing Agents: Effective Reinforcer for Thermal, Mechanical, and Flame-Retardant Properties of Polystyrene Nanocomposites," *ACS Applied Materials & Interfaces* 8 (2016): 26266–26274.
45. D. Janas, M. Rdest, and K. K. Koziol, "Flame-Retardant Carbon Nanotube Films," *Applied Surface Science* 411 (2017): 177–181.
46. K. M. Holder, R. J. Smith, and J. C. Grunlan, "A Review of Flame Retardant Nanocoatings Prepared Using Layer-by-Layer Assembly of Polyelectrolytes," *Journal of Materials Science* 52 (2017): 12923–12959.
47. H. Parsimehr, M. Enayati, and A. E. Langroudi, "Materials and Chemistry of Flame-Retardant Polyurethanes," in *Green Flame Retardants*, vol. 2 (ACS Publications, 2021), 47–63.

Supporting Information

Additional supporting information can be found online in the Supporting Information section.